Asymptotic Analysis of Narrow Escape Problems in Nonspherical Three-Dimensional Domains

Daniel Gomez [a)], Alexei F. Cheviakov [b)]

Department of Mathematics and Statistics, University of Saskatchewan, Saskatoon, S7N 5E6 Canada

Abstract

Narrow escape problems consider the calculation of the mean first passage time (MFPT) for a particle undergoing Brownian motion in a domain with a boundary that is everywhere reflecting except for at finitely many small holes. Asymptotic methods for solving these problems involve finding approximations for the MFPT and average MFPT that increase in accuracy with decreasing hole sizes. While relatively much is known for the two-dimensional case, the results available for general three-dimensional domains are rather limited. The present paper addresses the problem of finding the average MFPT for a class of three-dimensional domains bounded by the level surface of an orthogonal coordinate system. In particular, this class includes spheroids and other solids of revolution. The primary result presented is a two term asymptotic expansion for the average MFPT of such domains containing an arbitrary number of holes. Steps are taken towards finding higher order asymptotic expansions for both the average MFPT and the MFPT in these domains. The results for the average MFPT are compared to full numerical calculations performed with the COMSOL multiphysics FEM solver for three distinct domains - prolate and oblate spheroids and biconcave disks. This comparison shows good agreement with the proposed two-term expansion of the average MFPT in the three domains.

1 Introduction

Consider a bounded domain $\Omega \in \mathbb{R}^d$ $(d = 2, 3)$ whose boundary, $\partial\Omega$, is everywhere reflecting except at finitely many small absorbing windows, the collection of which is denoted by $\partial\Omega_a = \bigcup_{j=1}^{N} \partial\Omega_{\varepsilon_j}$ (see Fig. 1). Narrow escape problems are concerned with determining the behaviour of a particle undergoing Brownian motion which is enclosed within such a domain. In particular, the quantity of interest is the mean first passage time (MFPT), $v(x)$, which denotes the expectation value of the time it takes for such a particle starting at $x \in \Omega$ to escape the enclosing domain through one of the small absorbing windows, or traps, which are respectively characterized by

[a)] Electronic mail: dag857@mail.usask.ca

[b)] Corresponding author. Electronic mail: chevaikov@math.usask.ca

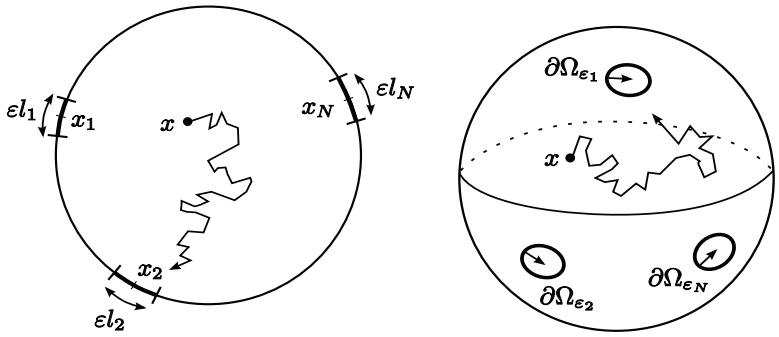

Figure 1: A Schematic of the narrow escape problem in a two- and a three-dimensional domain.

a length $|\partial\Omega_{\varepsilon_j}| = \mathcal{O}(\varepsilon)$ (in two dimensions) or an area $|\partial\Omega_{\varepsilon_j}| = \mathcal{O}(\varepsilon^2)$ (in three dimensions). Here $\varepsilon \ll 1$ is a small parameter, in terms of which, diam $(\Omega) = \mathcal{O}(1)$.

Narrow escape problems arise in the modeling of escape kinetics in chemistry [9], as well as in multiple cell-biological applications, such as receptor trafficking in a synaptic membrane [10], RNA transport from the cell nucleus through the nuclear pores [8], and others. An excellent review of applications involving narrow escape problems is provided in [1].

In a narrow escape problem, the MFPT can be expressed as the solution of the following Poisson equation with mixed Dirichlet-Neumann boundary conditions [14]:

$$\Delta v = -\frac{1}{D}, \qquad x \in \Omega, \tag{1a}$$

$$v(x) = 0, \qquad x \in \partial\Omega_a, \tag{1b}$$

$$\partial_n v(x) = 0, \qquad x \in \partial\Omega \setminus \partial\Omega_a, \tag{1c}$$

D being the diffusivity coefficient. An additional quantity that is of interest is the average MFPT $\bar{v}$, which describes the spatial average of the MFPT, and is given by

$$\bar{v} \equiv \frac{1}{|\Omega|} \int_\Omega v(x)\, dx. \tag{2}$$

For small trap sizes, the quantities $v(x)$ and $\bar{v}$ can be sought in terms of asymptotic series in terms of the dimensionless size parameter ε. As $\varepsilon \to 0$, the MFPT diverges, indicating that this problem is singularly perturbed.

Consideration of the narrow escape problem in two-dimensional domains has yielded numerous results for both the MFPT and the average MFPT. Results for the average MFPT in the case of a single absorbing window when the two-dimensional domain is bounded by a smooth curve, a non-smooth curve, or when the domain is a unit disk can be found in [10, 18, 15, 16]. Using a different approach the authors in [11] determined a higher order asymptotic expansion for an arbitrary two-dimensional domain with an arbitrary number of well separated absorbing windows. These asymptotic expansions are formulated in terms of the regular part of the surface Neumann Green's function for the domains. In the particular case of a unit disk and

unit square, where explicit analytic expressions for the surface Neumann Green's functions are known, explicit asymptotic expansions can be given as in [11].

The added complexity of three-dimensional domains has restricted the generality and accuracy of the results for the MFPT and average MFPT. In [17], the authors considered an arbitrary three-dimensional domain with a smooth boundary and a single circular absorbing window. By first finding an expression for the singular part of the corresponding surface Neumann Green's function, and then solving an integral equation, the authors of [17] determined a two-term asymptotic expansion for the average MFPT. Using similar methods to those found in [11], the authors of [4] were able to give a three-term asymptotic expansion for both the average MFPT and the MFPT for the unit sphere with an arbitrary number of well separated non-equal absorbing windows. A rigorous proof of some of the asymptotic results in [4] has been recently given in [2]. Applicability limits of asymptotic MFPT results for some two- and three-dimensional domains have been numerically studied in [3].

The higher-order term of the three-term asymptotic expansion for the spherical average MFPT is dependent on the trap sizes as well as mutual trap locations [4]. In particular, for N equal traps, the interaction term is proportional to the "interaction energy" given by a sum of Coulombic, logarithmic, and an additional regular pairwise interaction energies:

$$\mathcal{H}(x_1,\ldots,x_N)=\sum_{i=1}^{N}\sum_{j=i+1}^{N}\left(\frac{1}{|x_i-x_j|}-\frac{1}{2}\log|x_i-x_j|-\frac{1}{2}\log\left(2+|x_i-x_j|\right)\right). \tag{3}$$

Here x_i, $i=1,\ldots,N$, are Cartesian coordinate triples for the trap locations on the unit sphere.

A related global optimization problem arises, to minimize the average MFPT by optimizing boundary trap locations. This problem is a generalization of the famous Thomson problem for electrons on the unit sphere, interacting with a Coulomb potential. Except for special symmetric cases, exact optimal configurations of N particles on the surface of a unit sphere or any other three-dimensional domain are not known; finding them numerically presents a significant computational challenge due to the existence of numerous local minima. Extensive literature on the subject exists; see, e.g., [13, 6] and references therein. A number of putative optimal configurations of N equal traps minimizing the MFPT on the unit sphere have been computed in [4]. An asymptotic expression for the trap "interaction energy" for a unit sphere with N small traps of a common radius and N large traps of a common radius has been computed and numerically optimized in [3].

When the number of traps is large, $N \gg 1$, a dilute trap limit of homogenization theory can be used to replace the strongly heterogeneous Dirichlet-Neumann problem (1) with a spherically symmetric Robin problem for which an exact solution is readily found. The Robin problem boundary condition parameters for the case of the unit sphere have been asymptotically calculated in [5].

The primary objective of this paper is to extend the results of [17] and [4] to a wider class of three-dimensional domains, in particular, domains bounded by smooth surfaces that are coordinate surfaces of one of the coordinates of a general orthogonal coordinate set in three dimensions. Local stretched coordinates in the vicinity of a boundary point are considered in Section 2, and asymptotic expressions for the Laplacian and the surface Neumann Green's function are derived. These are used in the method of matched asymptotic expansions to compute the first two terms

of the average MFPT $\bar{v}$ for an arbitrary domain within the considered class (Principal Result 2.1). This is a direct generalization of the results of [17] onto the case of $N > 1$ traps, and the results of [4] onto non-spherical domains.

In Section 3, we compare the derived two-term asymptotic average MFPT for non-spherical domains with numerical results obtained using the COMSOL Multiphysics finite element solver. Comparisons are performed for several three-dimensional domains, and show good agreement for small trap sizes.

In Section 4, using certain assumptions for the far-field behaviour of one of the components of the asymptotic expansion, we show that the form of the higher-order asymptotic MFPT $v(x)$ within a domain in the considered class is similar to that of the unit sphere, in particular, it involves a higher-order term depending on mutual trap locations and the Green's function matrix. For the unit sphere, the MFPT formula reduces to the one known from [4].

A discussion of results and open problems is presented in Section 5.

2 Asymptotic Analysis of the MFPT Problem

We now wish to calculate an asymptotic MFPT expression for the narrow escape problem (1) for a class of three-dimensional domains Ω specified below. The smooth domain boundary $\partial\Omega$ will contains $N \geq 1$ small well-separated traps centered at x_j, $j = 1, ..., N$. We will assume that each trap has a circular projection onto the tangent plane to $\partial\Omega$ at x_j, and has a radius εa_j, with $\varepsilon \ll 1$, $a_j = \mathcal{O}(1)$. For the domain itself, it is assumed that $\operatorname{diam}\Omega = \mathcal{O}(1)$.

To perform the calculations, the method of matched asymptotic expansions will be applied, extending the work of [4] to the case of a non-spherical domain. We will derive and use explicit asymptotic expressions for the Laplacian and surface Neumann Green's function in local stretched coordinates near a boundary trap.

2.1 A General Class of Three-Dimensional Domains

Let (μ, ν, ω) be an orthogonal coordinate system in $\mathbb{R}^3$. In addition suppose that fixing μ and varying the remaining two coordinates in some specified range leads to a smooth closed bounded surface in $\mathbb{R}^3$. It is the interior of such a surface to which we will restrict Ω in our considerations. In particular, we will be considering Ω defined by

$$\Omega \equiv \{(\mu, \nu, \omega) \,|\, 0 \leq \mu \leq \mu_0,\, 0 \leq \nu \leq \nu_0,\, 0 \leq \omega \leq \omega_0\},$$
$$\partial\Omega \equiv \{(\mu, \nu, \omega) \,|\, \mu = \mu_0,\, 0 \leq \nu \leq \nu_0,\, 0 \leq \omega \leq \omega_0\}.$$

The restriction of domains Ω to this particular form allows the unit normal to the surface $\partial\Omega$ to be written as $\hat{n} = \hat{\mu}$ so that the normal derivative becomes $\partial_n|_{\partial\Omega} = \partial_\mu|_{\mu=\mu_0}$, where we have assumed that $\hat{\mu}$ is normalized. A general point in the domain Ω or on its surface $\partial\Omega$ will be denoted $x = (\mu, \nu, \omega)$.

Next, denoting the scale factors by $h_\mu(x)$, $h_\nu(x)$, $h_\omega(x)$ we define

$$h_{\mu_j} = h_\mu(x_j), \qquad h_{\nu_j} = h_\nu(x_j), \qquad h_{\omega_j} = h_\omega(x_j),$$

where $x_j = (\mu_j, \nu_j, \omega_j) \in \partial\Omega$, $j = 1, ..., N$, denote the centers of the boundary traps. Finally, we introduce the local stretched coordinates (centered at the j^{th} trap) which are defined by

$$\eta = -h_{\mu_j}\frac{\mu - \mu_j}{\varepsilon}, \qquad s_1 = h_{\nu_j}\frac{\nu - \nu_j}{\varepsilon}, \qquad s_2 = h_{\omega_j}\frac{\omega - \omega_j}{\varepsilon}. \tag{4}$$

In (4), the coordinate η is chosen to increase towards the inside of the domain.

The above-described class of three-dimensional domains includes spheres, ellipsoids, spheroids, and in general, all axially symmetric domains.

2.2 The Laplacian in Local Stretched Coordinates

We recall that for an orthonormal coordinate system (μ, ν, ω), the Laplacian is given by

$$\Delta\Psi = \frac{1}{h_\mu h_\nu h_\omega}\left[\frac{\partial}{\partial\mu}\left(\frac{h_\nu h_\omega}{h_\mu}\frac{\partial\Psi}{\partial\mu}\right) + \frac{\partial}{\partial\nu}\left(\frac{h_\mu h_\omega}{h_\nu}\frac{\partial\Psi}{\partial\nu}\right) + \frac{\partial}{\partial\omega}\left(\frac{h_\mu h_\nu}{h_\omega}\frac{\partial\Psi}{\partial\omega}\right)\right].$$

Converting to the local stretched coordinates defined in (4) and then expanding the Laplacian in terms of ε, one gets

$$\Delta = \frac{1}{\varepsilon^2}\Delta_{(\eta,s_1,s_2)} + \frac{1}{\varepsilon}\mathcal{L}_\Delta + \mathcal{O}(1), \tag{5}$$

where

$$\Delta_{(\eta,s_1,s_2)} \equiv \frac{\partial^2}{\partial\eta^2} + \frac{\partial^2}{\partial s_1^2} + \frac{\partial^2}{\partial s_2^2},$$

and

$$\mathcal{L}_\Delta \equiv \Lambda_\eta\frac{\partial^2}{\partial\eta^2} + \Lambda_{s_1}\frac{\partial^2}{\partial s_1^2} + \Lambda_{s_2}\frac{\partial^2}{\partial s_2^2} + \lambda_\eta\frac{\partial}{\partial\eta} + \lambda_{s_1}\frac{\partial}{\partial s_1} + \lambda_{s_2}\frac{\partial}{\partial s_2}.$$

A somewhat lengthy calculation involving the series expansion about $\varepsilon = 0$ shows that the λ coefficients are given by

$$\lambda_\eta = -\frac{1}{h_{\nu_j}h_{\omega_j}}\frac{\partial}{\partial\mu}\left(\frac{h_\nu h_\omega}{h_\mu}\right)\bigg|_{x_j}, \qquad \lambda_{s_1} = -\frac{1}{h_{\mu_j}h_{\omega_j}}\frac{\partial}{\partial\nu}\left(\frac{h_\mu h_\omega}{h_\nu}\right)\bigg|_{x_j},$$
$$\lambda_{s_2} = -\frac{1}{h_{\mu_j}h_{\nu_j}}\frac{\partial}{\partial\omega}\left(\frac{h_\mu h_\nu}{h_\omega}\right)\bigg|_{x_j}.$$

Similarly we find that each of the Λ coefficients can be expressed as a linear combination of η, s_1, and s_2. Explicitly, each of these coefficients can be written as

$$\Lambda_\alpha = \Lambda_\alpha^\eta\eta + \Lambda_\alpha^{s_1}s_1 + \Lambda_\alpha^{s_2}s_2, \qquad \alpha = \eta,\, s_1,\, s_2,$$

where

$$\Lambda_\eta^\eta = \frac{2}{h_{\mu_j}^2}\frac{\partial h_\mu}{\partial\mu}\bigg|_{x_j}, \qquad \Lambda_\eta^{s_1} = -\frac{2}{h_{\mu_j}h_{\nu_j}}\frac{\partial h_\mu}{\partial\nu}\bigg|_{x_j}, \quad \Lambda_\eta^{s_2} = -\frac{2}{h_{\mu_j}h_{\omega_j}}\frac{\partial h_\mu}{\partial\omega}\bigg|_{x_j},$$
$$\Lambda_{s_1}^\eta = \frac{2}{h_{\mu_j}h_{\nu_j}}\frac{\partial h_\nu}{\partial\mu}\bigg|_{x_j}, \quad \Lambda_{s_1}^{s_1} = -\frac{2}{h_{\nu_j}^2}\frac{\partial h_\nu}{\partial\nu}\bigg|_{x_j}, \qquad \Lambda_{s_1}^{s_2} = -\frac{2}{h_{\nu_j}h_{\omega_j}}\frac{\partial h_\nu}{\partial\omega}\bigg|_{x_j},$$
$$\Lambda_{s_2}^\eta = \frac{2}{h_{\mu_j}h_{\omega_j}}\frac{\partial h_\omega}{\partial\mu}\bigg|_{x_j}, \quad \Lambda_{s_2}^{s_1} = -\frac{2}{h_{\nu_j}h_{\omega_j}}\frac{\partial h_\omega}{\partial\nu}\bigg|_{x_j}, \quad \Lambda_{s_2}^{s_2} = -\frac{2}{h_{\omega_j}^2}\frac{\partial h_\omega}{\partial\omega}\bigg|_{x_j}.$$

2.3 The Surface Neumann Green's Function

The surface Neumann Green's function plays a critical role in the method of matched asymptotic expansions, which is used in the bulk of the upcoming analysis. The surface Neumann Green's function is defined for each trap $\partial\Omega_{\varepsilon_j}$ as the solution of the problem

$$\begin{aligned} \Delta G_s(x;x_j) &= \frac{1}{|\Omega|}, \qquad x \in \Omega, \\ \partial_n G_s(x;x_j) &= \delta_s(x-x_j), \qquad x \in \partial\Omega, \\ \int_\Omega G\,dx &= 0. \end{aligned} \tag{6}$$

Explicit analytic solutions to the problem (6) are not known for arbitrary domains Ω. However in the case of a unit sphere an explicit expression for the surface Neumann Green's function is available (see, e.g., [4]). It has the form

$$G_s(x;x_j) = \frac{1}{2\pi|x-x_j|} + \frac{1}{8\pi}\Big(|x|^2+1\Big) + \frac{1}{4\pi}\log\bigg(\frac{2}{1-|x|\cos\gamma+|x-x_j|}\bigg) - \frac{7}{10\pi}, \tag{7}$$

where γ is the angle between the vectors $x \in \Omega$ and $x_j \in \partial\Omega$, defined by $|x|\cos\gamma = x\cdot x_j$, $|x_j| = 1$.

For more general domains, the authors of [17] determined that the surface Neumann Green's function takes the form

$$G_s(x;x_j) = \frac{1}{2\pi|x-x_j|} - \frac{H(x_j)}{4\pi}\log|x-x_j| + v_s(x;x_j), \tag{8}$$

where $H(x_j)$ is the mean curvature of $\partial\Omega$ at x_j, and $v_s(x;x_j)$ is a bounded (but not necessarily regular) function of x and x_j in Ω.

In a similar procedure to that used for finding the approximate Laplacian in local stretched coordinated, we can obtain an asymptotic expression for the surface Neumann Green's function in local stretched coordinates. To do this, first observe that expansions about $\varepsilon = 0$ yield

$$\begin{aligned} \frac{1}{|x-x_j|} &= \frac{1}{\varepsilon\rho} + Y_D(\eta,s_1,s_2) + \mathcal{O}(\varepsilon), \\ \log|x-x_j| &= \log\varepsilon + \frac{1}{2}\log\rho + \mathcal{O}(\varepsilon), \end{aligned} \tag{9}$$

where $\rho = \sqrt{\eta^2+s_1^2+s_2^2}$. A lengthy calculation, based on the orthogonality of the coordinates (μ,ν,ω), shows that

$$Y_D(\eta,s_1,s_2) = \frac{1}{4\rho^3}\Big[\Lambda_\eta\eta^2 + \Lambda_{s_1}s_1^2 + \Lambda_{s_2}s_2^2 + \gamma_D\Big],$$

with γ_D a constant defined by

$$\gamma_D = 12\frac{\frac{\partial x}{\partial\mu}\cdot\frac{\partial^2 x}{\partial\nu\partial\omega}}{h_{\mu_j}h_{\nu_j}h_{\omega_j}}\bigg|_{x_j} = 12\frac{\frac{\partial x}{\partial\nu}\cdot\frac{\partial^2 x}{\partial\mu\partial\omega}}{h_{\mu_j}h_{\nu_j}h_{\omega_j}}\bigg|_{x_j} = 12\frac{\frac{\partial x}{\partial\omega}\cdot\frac{\partial^2 x}{\partial\mu\partial\nu}}{h_{\mu_j}h_{\nu_j}h_{\omega_j}}\bigg|_{x_j}.$$

It remains to put these expansions together with the expansion of the bounded unknown function v_s. Based on the boundedness of $v_s(x;x_j)$ for x and x_j in Ω as well as the coordinate transformations given in (4), and the known result for the unit sphere, we pose the following asymptotic expansion for v_s:

$$v_s(x;x_j) = b_0(\eta,s_1,s_2) + g_1(\eta,s_1,s_2)\varepsilon\log\frac{\varepsilon}{2} + \mathcal{O}(\varepsilon).$$

With this, the surface Neumann Green's function becomes

$$\begin{aligned} G_s(\eta,s_1,s_2) =& \frac{1}{2\pi\rho}\frac{1}{\varepsilon} - \frac{H(x_j)}{4\pi}\log\frac{\varepsilon}{2} + g_0(\eta,s_1,s_2) \\ &+ g_1(\eta,s_1,s_2)\varepsilon\log\frac{\varepsilon}{2} + \mathcal{O}(\varepsilon), \end{aligned} \tag{10}$$

where

$$g_0(\eta,s_1,s_2) = \frac{1}{2\pi}Y_D(\eta,s_1,s_2) + \frac{H(x_j)}{8\pi}\log\frac{\rho}{4} + b_0(\eta,s_1,s_2).$$

It is worthwhile to note that for the unit sphere the results in [4] indicate that

$$\begin{aligned} g_0 &= \frac{1}{4\pi}\left[\frac{\eta(s_1^2+s_2^2)}{\rho^3} - \frac{s_1^2 s_2\cot\theta_j}{\rho^3}\right] - \frac{1}{4\pi}\log(\rho+\eta) - \frac{9}{20\pi}, \\ g_1 &= 0, \end{aligned}$$

where θ_j is the spherical polar angle of the trap position x_j.

2.4 Matched Asymptotic Expansion Solution of the MFPT Problem

The method of matched asymptotic expansions is now used to compute an approximation for the solution $v(x)$ of the narrow escape problem (1) in domains Ω specified in Section 2.1.

Consider N small traps centered at the points x_j on the domain boundary, $j = 1,...,N$. For a point $x \in \Omega$ far from each of the boundary traps x_j, $|x-x_j| = \mathcal{O}(1)$, define the outer asymptotic expansion for the MFPT $v(x)$:

$$v \sim \frac{1}{\varepsilon}v_0 + v_1 + \varepsilon\log\frac{\varepsilon}{2}v_2 + \varepsilon v_3 + \cdots. \tag{11}$$

Substitution of (11) into the problem (1) yields

$$\Delta v_k = -\frac{1}{D}\delta_{k1}, \qquad x\in\Omega; \qquad \partial_n v_k = 0, \qquad x \in \partial\Omega\setminus\{x_1,...,x_N\}, \tag{12}$$

where $k = 0,1,2,\ldots$, and δ_{ij} denotes the Kronecker delta symbol. In a similar way, when $x \in \Omega$ is close to a trap x_j, we pose the inner asymptotic MFPT expansion

$$v(x) = w(\eta,s_1,s_2) \sim \frac{1}{\varepsilon}w_0 + \log\frac{\varepsilon}{2}w_1 + w_2 + \cdots, \tag{13}$$

using the local stretched coordinates (η, s_1, s_2). Substituting this expression into (1) and this time using the local form of the Laplacian given by (5), we obtain for $k = 0, 1, 2, \ldots$,

$$\begin{aligned} \Delta_{(\eta,s_1,s_2)} w_k &= -\delta_{k2} \mathcal{L}_\Delta w_0, & \eta \geq 0, \qquad & s_1, s_2 \in \mathbb{R}, \\ \partial_\eta w_k &= 0, & \eta = 0, \qquad & s_1^2 + s_2^2 \geq a_j^2, \\ w_k &= 0, & \eta = 0, \qquad & s_1^2 + s_2^2 \leq a_j^2. \end{aligned} \tag{14}$$

The inner expansion (13) is matched with the outer expansion (11) by imposing the matching condition $v \sim w$, or explicitly,

$$\frac{1}{\varepsilon} v_0 + v_1 + \varepsilon \log \frac{\varepsilon}{2} v_2 + \varepsilon v_3 + \cdots \sim \frac{1}{\varepsilon} w_0 + \log \frac{\varepsilon}{2} w_1 + w_2 + \cdots . \tag{15}$$

where the left- and right-hand sides must agree as $x \to x_j$ and as $\rho = \sqrt{\eta^2 + s_1^2 + s_2^2} \to \infty$.

The leading order matching condition is $w_0 \sim v_0$ as $\rho \to \infty$; this is satisfied by the form

$$w_0 = v_0(1 - w_c),$$

(see [4] for details), where w_c is the solution to the electrified disk problem

$$\begin{aligned} \Delta_{(\eta,s_1,s_2)} w_c &= 0, & \eta \geq 0, \qquad & s_1, s_2 \in \mathbb{R} \\ \partial_\eta w_c &= 0, & \eta = 0, \qquad & s_1^2 + s_2^2 \geq a_j^2, \\ w_c &= 1, & \eta = 0, \qquad & s_1^2 + s_2^2 \leq a_j^2. \end{aligned}$$

The solution to this problem is explicitly known to be given by

$$w_c = \frac{2}{\pi} \sin^{-1}\left(\frac{a_j}{L}\right), \tag{16}$$

where

$$L(\eta, \sigma) \equiv \frac{1}{2}\left([(\sigma + a_j)^2 + \eta^2]^{1/2} + [(\sigma - a_j)^2 + \eta^2]^{1/2} \right), \qquad \sigma \equiv (s_1^2 + s_2^2)^{1/2}.$$

Expanding as $\rho \to \infty$, we obtain the far-field behaviour of w_c as $\rho \to \infty$:

$$w_c \sim \frac{2a_j}{\pi}\left(\frac{1}{\rho} + \frac{a_j^2}{6}\left(\frac{1}{\rho^3} - \frac{3\eta^2}{\rho^5} \right) + \cdots \right).$$

For convenience, define the trap 'capacitance' $c_j \equiv 2a_j/\pi$. The far-field behaviour of w_0 as $\rho \to \infty$ is consequently given by

$$w_0 \sim v_0\left(1 - \frac{c_j}{\rho} + \mathcal{O}(\rho^{-3}) \right).$$

Substituting this result into (15), we have

$$\frac{1}{\varepsilon}v_0 + v_1 + \varepsilon\log\frac{\varepsilon}{2}v_2 + \varepsilon v_3 + \cdots \sim \frac{1}{\varepsilon}v_0\left(1 - \frac{c_j}{\rho} + \mathcal{O}(\rho^{-3})\right) + \log\frac{\varepsilon}{2}w_1 + w_2 + \cdots .$$

Using (9), we find that the ρ^{-1} terms contribute $\varepsilon/|x - x_j|$, so that the next leading order matching condition above gives $v_1 \sim -v_0 c_j/|x - x_j|$ as $x \to x_j$ $(j = 1, ..., N)$. This singular behaviour of v_1 near each x_j can be expressed as

$$\Delta v_1 = -\frac{1}{D}, \qquad x \in \Omega; \qquad \partial_\mu|_{\mu_0} v_1 = -2\pi v_0 \sum_{i=1}^{N} \frac{c_i}{h_{\nu_i} h_{\omega_i}} \delta(\nu - \nu_i)\delta(\omega - \omega_i).$$

Applying the divergence theorem to ∇v_1, we obtain

$$-\frac{|\Omega|}{D} = \iiint_\Omega \nabla\cdot(\nabla v_1)\, dV = \oiint_{\partial\Omega} \partial_n v_1\, dA = -2\pi v_0 \sum_{i=1}^{N} c_i,$$

and hence

$$v_0 = \frac{|\Omega|}{2\pi D N \bar{c}}. \tag{17}$$

In (17), $\bar{c} = \sum_{i=1}^{N} c_i$ is the average trap capacitance.

Further, with reference to (6), one observes that v_1 can be expressed as a superposition of surface Neumann Green's functions as

$$v_1 = -2\pi v_0 \sum_{i=1}^{N} c_i G_s(x; x_i) + \chi, \tag{18}$$

where χ is an unknown integration constant. Using the local form of the Green's function (10), the behaviour of v_1 near x_j is determined to be given by

$$\begin{aligned} v_1 \sim -\frac{c_j v_0}{\rho}\frac{1}{\varepsilon} + \frac{c_j H(x_j) v_0}{2}\log\frac{\varepsilon}{2} - 2\pi v_0 c_j g_0 \\ - 2\pi v_0 c_j g_1 \varepsilon \log\frac{\varepsilon}{2} + B_j + \chi, \end{aligned}$$

where $B_j = -2\pi v_0 \sum_{i\neq j} c_i G_s(x_j; x_i)$. With this near field expansion, the matching condition (15) near x_j now reads

$$\begin{aligned} \frac{1}{\varepsilon}v_0\left(1 - \frac{c_j}{\rho}\right) + \frac{v_0 c_j H(x_j)}{2}\log\frac{\varepsilon}{2} - 2\pi v_0 c_j g_0 + B_j + \chi \\ +(v_2 - 2\pi v_0 c_j g_1)\varepsilon\log\frac{\varepsilon}{2} + \varepsilon v_3 \sim \frac{1}{\varepsilon}v_0\left(1 - \frac{c_j}{\rho} + \mathcal{O}(\rho^{-3})\right) + w_1\log\frac{\varepsilon}{2} + w_2 + \cdots , \end{aligned} \tag{19}$$

from which we deduce the far field behaviour for w_1 as $\rho \to \infty$ to be

$$w_1 \sim \frac{v_0 c_j H(x_j)}{2}.$$

Up to the multiplicative factor of $H(x_j)$, the above far-field behaviour is identical to that encountered in [4] for the unit sphere, where the mean curvature at each trap center $H(x_j) \equiv 1$. Parallel to [4], such an expansion leads to a problem in v_2 with no solutions. This can be fixed by inserting a constant term of order $\mathcal{O}(\log \varepsilon)$ between v_0 and v_1 in the outer expansion (11), as follows:

$$\chi = \chi_0 \log \frac{\varepsilon}{2} + \chi_1,$$

where χ_0, χ_1 are unknown constants independent of ε. This leads to the far-field behaviour

$$w_1 \sim \frac{v_0 c_j H(x_j)}{2} + \chi_0$$

as $\rho \to \infty$.

The next step is to express w_1 in terms of the solution to the electrified disk problem w_c, as it was done for w_0:

$$w_1 = \left(\chi_0 + \frac{v_0 c_j H(x_j)}{2}\right)(1 - w_c).$$

Thus the far-field behaviour of w_c yields the far field behaviour of w_1:

$$w_1 \sim \left(\chi_0 + \frac{v_0 c_j H(x_j)}{2}\right)\left(1 - \frac{c_j}{\rho} + \mathcal{O}(\rho^{-3})\right).$$

The ρ^{-1} term gives an ε term with coefficient of $1/|x - x_j|$, which yields an $\varepsilon \log \frac{\varepsilon}{2}$ term in the right hand side of the matching condition. With reference to the latest result in the matching condition above, this yields the following condition on v_2 as $x \to x_j$:

$$v_2 - 2\pi v_0 c_j g_1 \sim -\left(\chi_0 + \frac{v_0 c_j H(x_j)}{2}\right)\frac{c_j}{|x - x_j|}.$$

To proceed with the analysis, more information about $g_1(\eta, s_1, s_2)$ is needed. As discussed earlier, for the sphere it was observed in [4] that there is no $\varepsilon \log \frac{\varepsilon}{2}$ term in the near-field expansion of the surface Neumann-Green's function (i.e. $g_1 \equiv 0$). This leads us make the following key assumption.

Key Assumption 1: The g_1 term in the local expansion of the surface Neumann Green's function is identically zero.

The above assumption is motivated by the explicit form of the surface Neumann Green's function for the unit sphere, and is supported by the numerical results in Section 3.

Using the above expansion, we can rewrite the problem for v_2 in distributional form as

$$\Delta v_2 = 0, \qquad x \in \Omega;$$

$$\partial_\mu|_{\mu_0} v_2 = -2\pi \sum_{i=1}^{N} \left(\chi_0 + \frac{v_0 c_i H(x_i)}{2}\right)\frac{c_i}{h_{\nu_1} h_{\omega_i}} \delta(\nu - \nu_i)\delta(\omega - \omega_i).$$

Applying the divergence theorem to ∇v_2 we find that

$$\chi_0 = -\frac{v_0}{2N\bar{c}} \sum_{i=1}^{N} c_i^2 H(x_i). \tag{20}$$

The solution v_2 can then be expressed as a superposition of the surface Neumann Green's function as

$$v_2 = -2\pi \sum_{i=1}^{N} c_i \left(\chi_0 + \frac{v_0 c_i H(x_i)}{2} \right) G_s(x; x_i) + \chi_2,$$

where χ_2 is an unknown constant.

Noting that the average value of each Green's function $G_s(x; x_j)$ is zero, it follows from averaging the outer expansion (11) that the leading terms of the average asymptotic MFPT are given by

$$\bar{v} \sim \frac{v_0}{\varepsilon} + \chi_0 \log \frac{\varepsilon}{2},$$

with v_0, χ_0 given by (17) and (20), respectively. With this, we have obtained the following result.

Principal Result 2.1. In the limit $\varepsilon \to 0$, the asymptotic approximation to the average MFPT is given in the outer region $|x - x_j| \gg \mathcal{O}(\varepsilon)$ by

$$\bar{v} = \frac{|\Omega|}{2\pi D N \bar{c} \varepsilon} \left(1 - \frac{1}{2N\bar{c}} \sum_{i=1}^{N} c_i^2 H(x_i) \varepsilon \log \frac{\varepsilon}{2} + \mathcal{O}(\varepsilon) \right), \tag{21}$$

where $H(x_i)$ is the mean curvature of the domain boundary $\partial\Omega$ at the center of the i^{th} trap.

3 Comparison of Numerical and Asymptotic Solutions

We now check the validity of the average MFPT expression (21), using the COMSOL Multiphysics 4.3b finite element solver to obtain numerical results for the average MFPT for three distinct geometries, with $N = 3$ and $N = 5$ traps. The three domains considered are an oblate spheroid, a prolate spheroid, and a biconcave disk – a blood cell-shaped axially symmetric domain. The comparison is made by considering the relative error given by

$$\text{R.E.} = 100\% \times |\bar{v}_{\text{numerical}} - \bar{v}_{\text{asymptotic}}| / \bar{v}_{\text{numerical}} \tag{22}$$

for various values of ε. In this expression, $\bar{v}_{\text{numerical}}$ refers to the results obtained using COMSOL, while $\bar{v}_{\text{asymptotic}}$ is given by (21).

We start from a discussion of the meshing, followed by a section outlining the geometry and results for each of the three domain geometries.

3.1 Mesh Refinement

COMSOL Multiphysics 4.3b contains predefined mesh preferences varying from extremely coarse to extremely fine. These preferences vary the maximum element size, minimum element size, maximum element growth rate, resolution of curvature, as well as resolution of curvature. For the numerical simulation we used a free tetrahedral mesh which was *etremely fine* in a cylinder of radius 0.25 and depth between 0.14 and 0.125 centered at each trap, and *fine* mesh in the other regions. This mesh refinement strategy is illustrated in Figure 2.

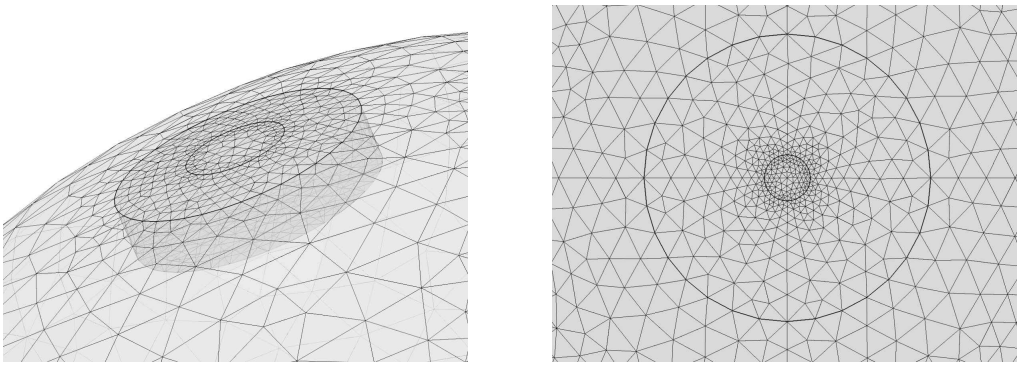

(a) (b)

Figure 2: Illustration of extremely fine and fine mesh regions.

3.2 Oblate Spheroid

As our first numerical example we consider the oblate spheroidal coordinates

$$x = \rho\cosh\xi\cos\nu\cos\phi, \qquad y = \rho\cosh\xi\cos\nu\sin\phi, \qquad z = \rho\sinh\xi\sin\nu, \tag{23}$$

where $\xi \in [0,\infty)$, $\nu \in [-\pi/2,\pi/2]$, and $\phi \in [0,2\pi)$. The orthogonality of such a coordinate system is easily verified. Furthermore the level sets $\xi = \xi_0$ generate oblate spheroids with a minor-axis of length $\rho\sinh\xi_0$ along the z-axis and a major-axis of length $\rho\cosh\xi_0$ on the xy-plane. The volume enclosed within $\xi \leq \xi_0$ therefore falls into our class of three-dimensional domains.

With $\xi_0 = \tanh^{-1}(0.5)$ and $\rho = (\cosh\xi_0)^{-1}$ the level surface $\xi = \xi_0$ becomes an oblate spheroid with major-axis of length 1 and minor-axis of length 0.5. Explicitly, the surface is parametrized by

$$x = \cos\nu\cos\phi, \qquad y = \cos\nu\sin\phi, \qquad z = 0.5\cdot\sin\nu. \tag{24}$$

The volume of this oblate spheroid is $|\Omega| = 2.0944$ and its mean curvature is given by

$$H(\nu) = 0.5\frac{8-3\cos^2\nu}{(4-3\cos^2\nu)^{3/2}}. \tag{25}$$

The trap configurations and relative radii for both $N = 3$ and $N = 5$ are shown in Table 1. The comparisons between the COMSOL numerical average MFPT and the asymptotic two-term formula (21) are shown in Figures 3 and 4 for the three- and the five-trap configurations, respectively. In addition to these plots, Figures 5a and 5b show the fully numerical calculation of the MFPT done in COMSOL to demonstrate the trap arrangements, as well as the MFPT behaviour on the boundary of the domain.

Number of Traps	a	ν	ϕ
$N = 3$	1	$-3\pi/8$	0
	2	0	π
	4	$\pi/2$	0
$N = 5$	1	0	$\pi/2$
	2	$\pi/4$	0
	2	$-\pi/2$	0
	3	$-\pi/4$	$\pi/4$
	4	$\pi/4$	π

Table 1: Trap locations and relative radii for in sample MFPT computations for oblate and prolate spheroids.

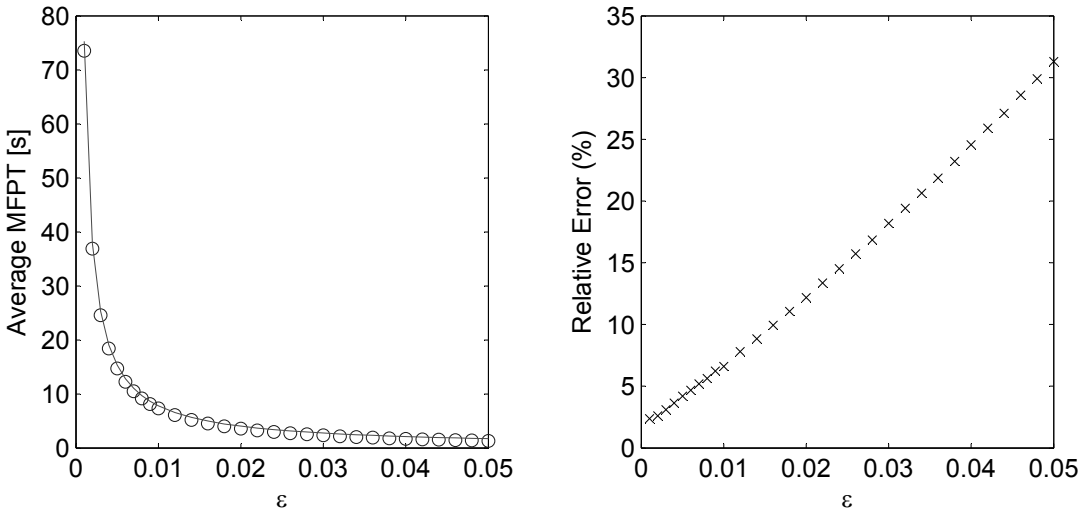

(a) (b)

Figure 3: Plots of (a) comparison of numerical (circles) and two-term asymptotic expression for average MFPT, and (b) relative error (see (22)) for an oblate spheroid with $N = 3$.

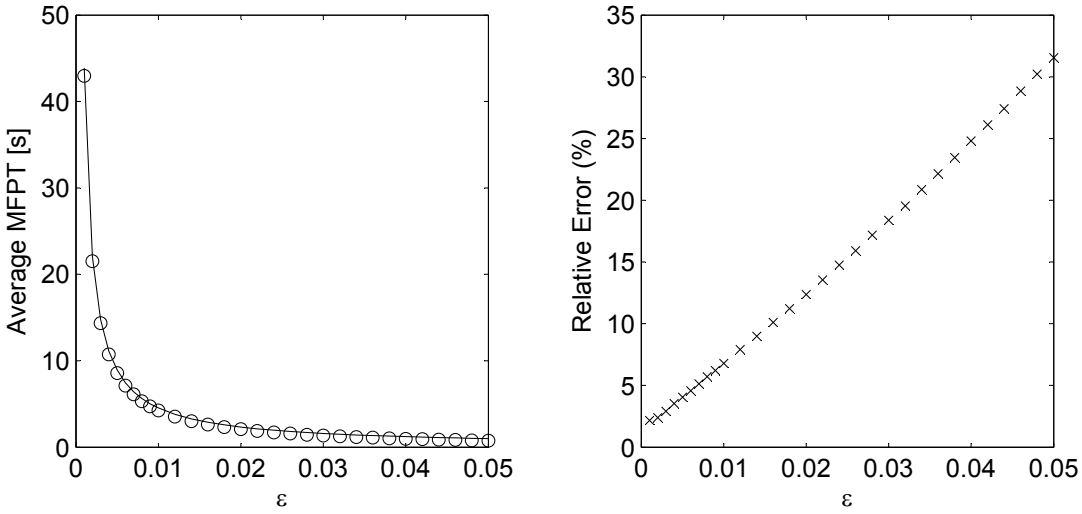

(a) (b)

Figure 4: Plots of (a) comparison of numerical (circles) and two-term asymptotic expression for average MFPT, and (b) relative error (see (22)) for an oblate spheroid with $N = 5$.

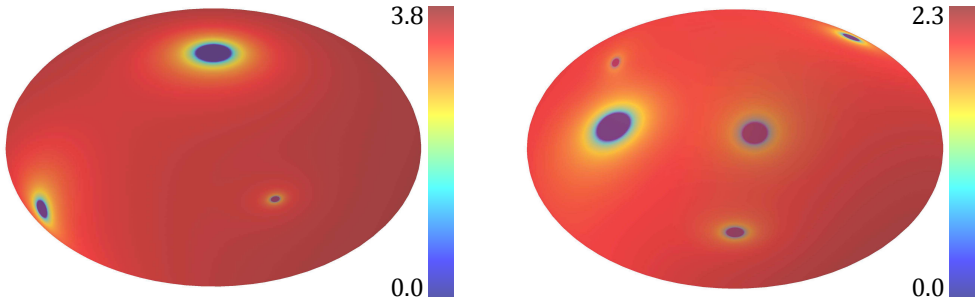

(a) (b)

Figure 5: Three-dimensional (transparent) plots of the numerical MFPT for the oblate spheroid at $\varepsilon = 0.02$ with (a) $N = 3$ and (b) $N = 5$ traps. The trap parameters are given in Table 1.

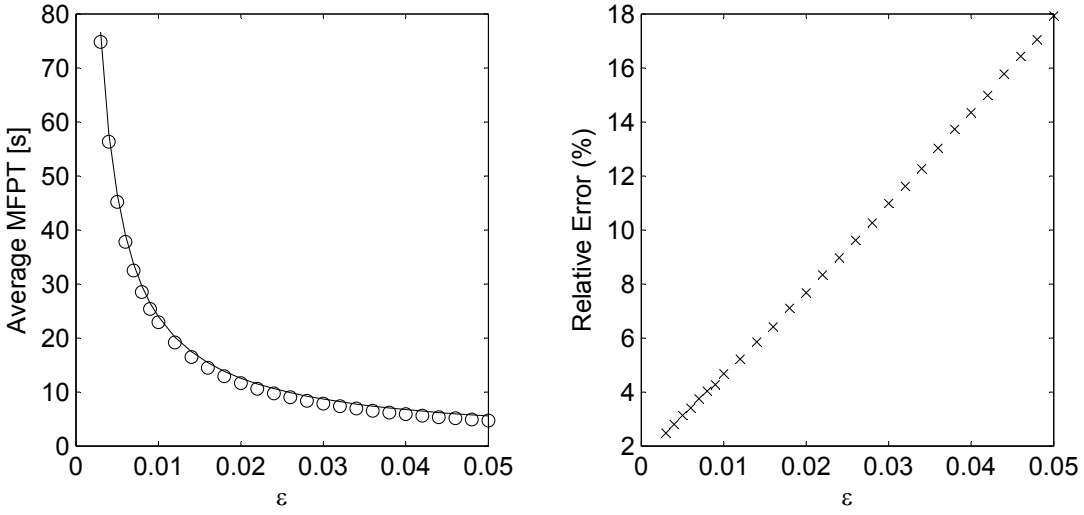

(a) (b)

Figure 6: Plots of (a) comparison of numerical (circles) and two-term asymptotic expression for average MFPT, and (b) relative error (see (22)) for a prolate spheroid with $N = 3$.

3.3 Prolate Spheroid

In a similar fashion to the oblate spheroid we can consider the prolate spheroidal coordiantes

$$x = \rho \sinh\xi \cos\nu \cos\phi, \qquad y = \rho \sinh\xi \cos\nu \sin\phi, \qquad z = \rho \cosh\xi \sin\nu, \tag{26}$$

where $\xi \in [0, \infty)$, $\nu \in [-\pi/2, \pi/2]$, and $\phi \in [0, 2\pi)$. As with the oblate spheroidal coordinates, the volume enclosed by $\xi \leq \xi_0$ falls within our class of three-dimensional domains.

With $\xi_0 = \tanh^{-1}(1/1.5)$ and $\rho = (\sinh\xi_0)^{-1}$ the level surface $\xi = \xi_0$ becomes a prolate spheroid with major-axis of length 1.5 and minor axis of length 1. The surface is parametrized by

$$x = \cos\nu \cos\phi, \qquad y = \cos\nu \sin\phi, \qquad z = 1.5 \cdot \sin\nu. \tag{27}$$

Finally it has a volume of $|\Omega| = 6.2832$ and a mean curvature given by

$$H(\nu) = 1.5 \frac{8 + 5\cos\nu^2}{(4 + 5\cos\nu^2)^{3/2}}. \tag{28}$$

The trap configurations and relative radii for both $N = 3$ and $N = 5$ are shown in Table 1. The comparisons between the COMSOL numerical average MFPT and the asymptotic two-term formula (21) are shown in Figures 6 and 7 for the $N = 3$ and $N = 5$ configurations respectively. Additionally, Figures 8a and 8b show the fully numerical calculation of the MFPT perfomed in COMSOL.

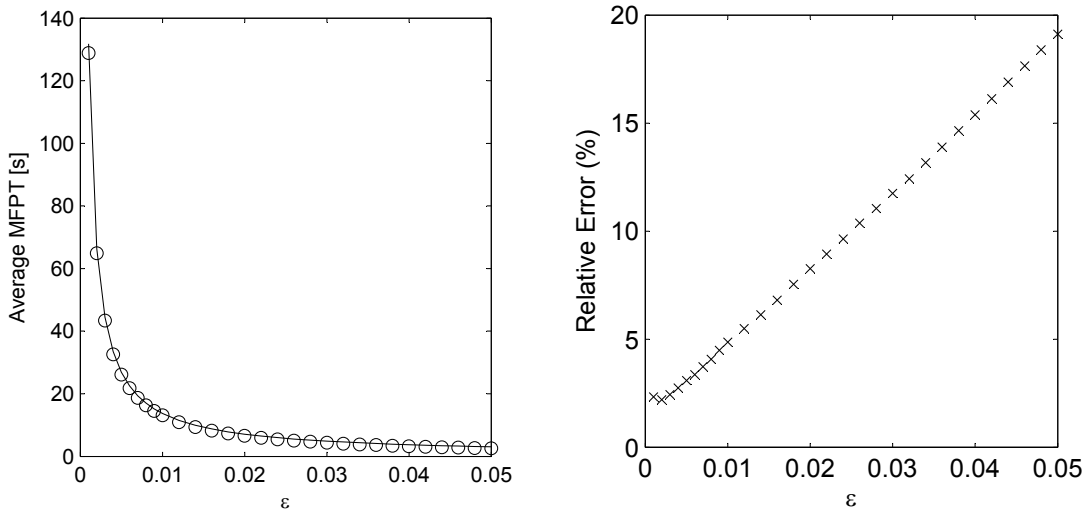

(a) (b)

Figure 7: Plots of (a) comparison of numerical (circles) and two-term asymptotic expression for average MFPT, and (b) relative error (see (22)) for a prolate spheroid with $N = 5$.

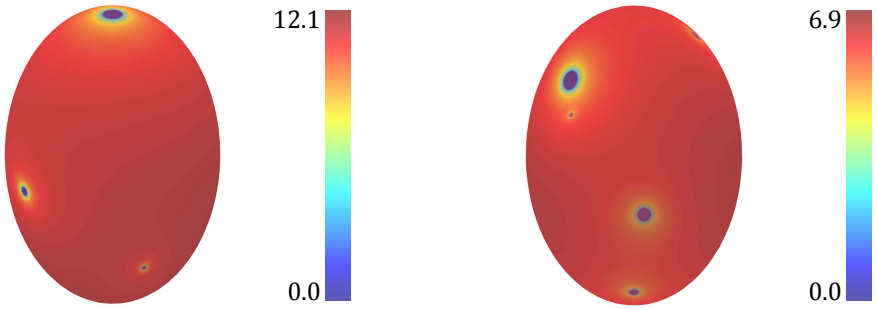

(a) (b)

Figure 8: Three-dimensional (transparent) plots of the numerically calculated MFPT (in seconds) for the prolate spheroid at $\varepsilon = 0.02$ with (a) $N = 3$ and (b) $N = 5$ traps.

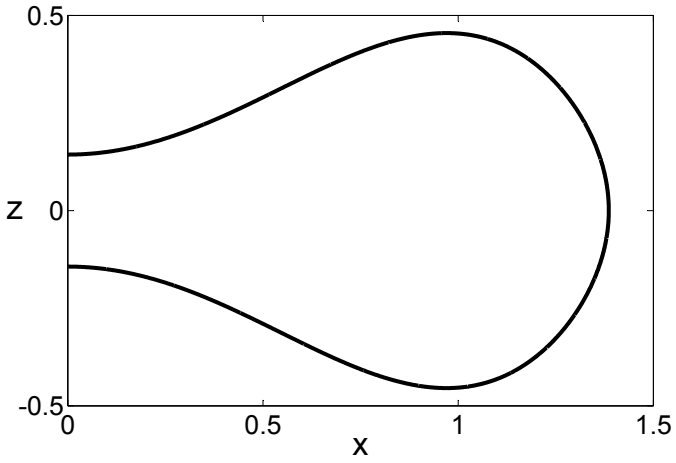

Figure 9: Biconcave disk cross-sectional view.

3.4 Biconcave Disk (Blood Cell)

The final example to be considered is the biconcave disk, which models the shape of blood cells, as discussed, for example, in [12]. This shape is obtained by rotating the curve

$$x = a\alpha \sin\chi, \qquad z = a\frac{\alpha}{2}(b + c\sin^2\chi - d\sin^4\chi)\cos\chi, \tag{29}$$

about the z axis. Here $\chi \in [0, \pi]$ with $\chi = 0, \pi/2, \pi$ corresponding to the north pole, the equator, and the south pole of the biconcave disk respectively (see Figure 9).

In general, an axially symmetric domain with a smooth boundary can be viewed as a coordinate level set in an orthogonal curvilinear coordinate system. One of the coordinates of that system is the azimuthal angle ϕ. If the desired domain boundary is given by $F(r, z) = \xi_0$ in cylindrical coordinates, with a necessary number of derivatives of F by r vanishing at $r = 0$, the three orthogonal coordinates are (ξ, ϕ, η), where ξ, η are defined in the (r, z) plane and are given by $\xi = F(r, z)$ and $\eta = G(r, z)$. The latter satisfies a linear homogeneous equation $\nabla F(r, z) \cdot \nabla G(r, z) = F_r G_r + F_z G_z = 0$. Setting $\xi \le \xi_0$ generates the axially symmetric domain Ω.

Including the rotation about the z axis, the surface parametrization of the biconcave disk is given by

$$x = a\alpha \sin\chi\cos\phi, \qquad y = a\alpha\sin\chi\sin\phi, \qquad z = a\frac{\alpha}{2}(b + c\sin^2\chi - d\sin^4\chi)\cos\chi, \tag{30}$$

where $\phi \in [0, 2\pi)$. Keeping the conventions of [12], we pick the parameters appearing in (29) to be

$$a = 1, \qquad \alpha = 1.38581994, \qquad b = 0.207, \qquad c = 2.003, \qquad d = 1.123.$$

The locations of each of the traps as well as their relative radii are given in Table 2. The

Number of Traps	a	χ	ϕ
$N = 3$	1	0	0
	2	$3\pi/4$	0
	4	$\pi/2$	π
$N = 5$	1	0	0
	2	$3\pi/4$	0
	2	π	0
	2	$\pi/2$	$\pi/2$
	4	$\pi/2$	π

Table 2: Trap locations and relative radii for biconcave disk (blood cell).

volume of the biconcave disk is readily calculated using (29); it is found to be

$$4\pi\left(\frac{1}{6}a^3\alpha^3 b + \frac{1}{15}ca^3\alpha^3 - \frac{4}{105}da^3\alpha^3\right).$$

The mean curvature calculation is simple but technical; it is accomplished using the parametrization (30). The comparisons between the COMSOL numerical average MFPT and that given by the two-term asymptotic expansion (21) are shown in Figures 10 and 11 for $N = 3$ and $N = 5$, respectively. Figures 12a and 12b show the fully numerical calculation of the MFPT with COMSOL, demonstrating the trap arrangements as well as the MFPT behaviour.

4 Towards Higher-Order Asymptotics

To obtain a third-order asymptotic expansion for the MFPT and the average MFPT, we need to determine the value of χ_1. Substituting the updated χ values into the matching condition (19), we find that w_2 has the far-field behaviour

$$w_2 \sim -2\pi v_0 c_j g_0 + B_j + \chi_1.$$

The problem for w_2 is further formulated in Appendix A. For the unit sphere, in [4], it is solved using

$$w_2 = (B_j + \chi_1)(1 - w_c) + \tilde{w}_2, \tag{31}$$

where $\tilde{w}_2$ is assumed to have the far-field behaviour

$$\tilde{w}_2 \sim \frac{v_0 b_j}{\rho}. \tag{32}$$

Under the same assumption, in a similar way as it was done for w_1 and v_2, the matching condition (15) yields

$$v_3 \sim -\frac{c_j(B_j + \chi_1) - v_0 b_j}{|x - x_j|} \qquad \text{as } x \to x_j, \qquad j = 1, \ldots, N.$$

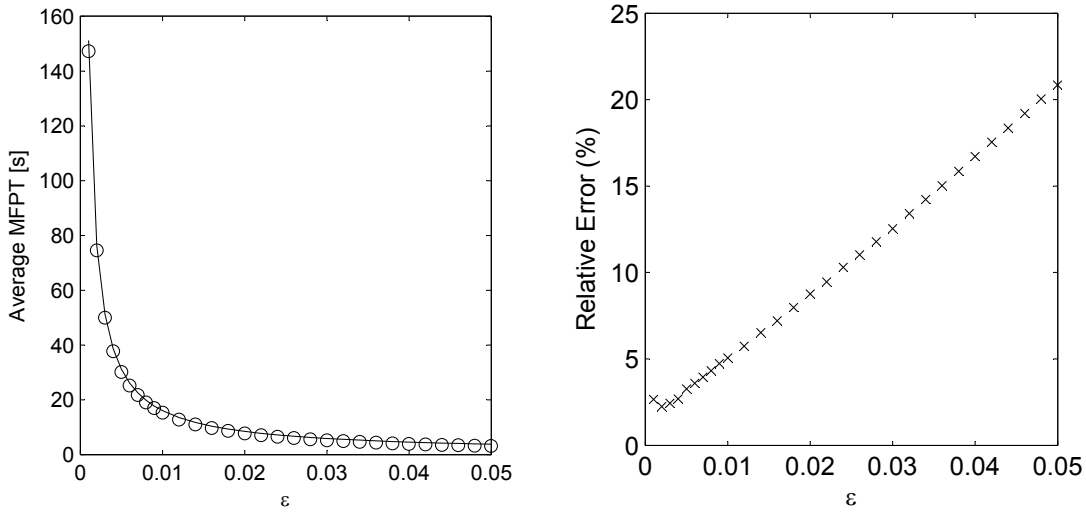

(a) (b)

Figure 10: Plots of (a) comparison of numerical (circles) and two-term asymptotic expression for average MFPT, and (b) relative error (see (22)) for a biconcave disk with $N = 3$.

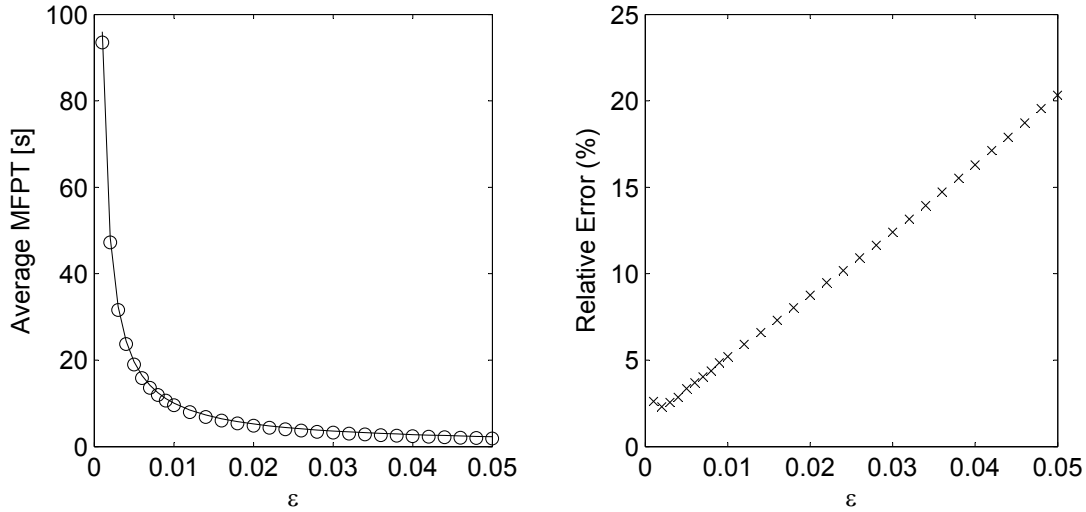

(a) (b)

Figure 11: Plots of (a) comparison of numerical (circles) and two-term asymptotic expression for average MFPT, and (b) relative error (see (22)) for a biconcave disk with $N = 5$.

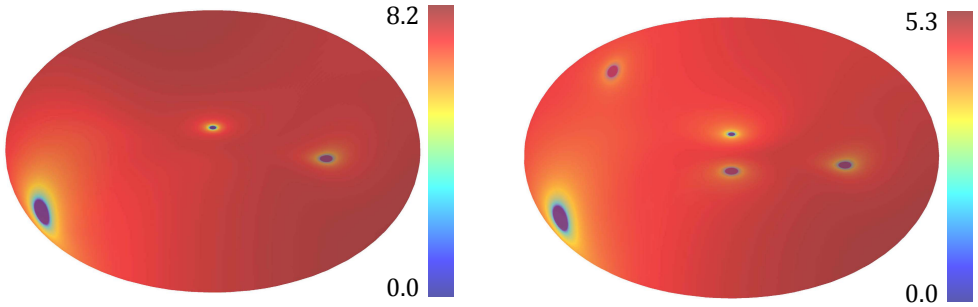

(a) (b)

Figure 12: Three-dimensional (transparent) plots of the numerically calculated MFPT (in seconds) for the biconcave disk (blood cell) at $\varepsilon = 0.02$ with (a) $N = 3$ and (b) $N = 5$ traps.

In distributional form, this leads to the problem

$$\Delta v_3 = 0, \qquad x \in \Omega; \qquad \partial_\mu v_3|_{\mu_0} = -2\pi \sum_{j=1}^{N} \Big[c_j(B_j + \chi_1) - v_0 b_j \Big] \frac{1}{h_{\nu_j} h_{\omega_j}} \delta(\nu - \nu_j)\delta(\omega - \omega_j).$$

Applying the divergence theorem to ∇v_3, one has

$$\chi_1 = \frac{1}{N\bar{c}} \bigg(v_0 \sum_{j=1}^{N} b_j - \sum_{j=1}^{N} c_j B_j \bigg).$$

Putting together the results for v_0 and v_1, we arrive at the following conjectured results.

Conjecture 4.1. In the outer region $|x - x_j| \gg \mathcal{O}(\varepsilon)$, the MFPT and the average MFPT for the problem (1) have the following asymptotic expressions:

$$\begin{aligned} v(x) = \frac{|\Omega|}{2\pi\varepsilon D N\bar{c}} \bigg[1 - \frac{1}{2N\bar{c}} \sum_{j=1}^{N} c_j^2 H(x_j) \varepsilon \log\frac{\varepsilon}{2} - 2\pi\varepsilon \sum_{j=1}^{N} c_j G_s(x; x_j) \\ + \frac{\varepsilon}{N\bar{c}} \sum_{j=1}^{N} b_j + \frac{2\pi\varepsilon}{N\bar{c}} \sum_{j=1}^{N} \sum_{i\neq j} c_j c_i G_s(x_j; x_i) + \mathcal{O}(\varepsilon^2 \log\varepsilon) \bigg], \end{aligned} \tag{33}$$

and

$$\bar{v} = \frac{|\Omega|}{2\pi\varepsilon D N\bar{c}} \bigg[1 - \frac{1}{2N\bar{c}} \sum_{j=1}^{N} c_j^2 H(x_j) \varepsilon \log\frac{\varepsilon}{2} + \frac{\varepsilon}{N\bar{c}} \bigg(\sum_{j=1}^{N} b_j + 2\pi \sum_{j=1}^{N} \sum_{i\neq j} c_j c_i G_s(x_j; x_i) \bigg) + \mathcal{O}(\varepsilon^2 \log\varepsilon) \bigg] \tag{34}$$

The above expressions are in rather similar to the ones for the unit sphere obtained in [4]. In particular, the "interaction energy"

$$p_c(x_1, \ldots, x_N) \equiv \sum_{j=1}^{N} \sum_{i\neq j} c_j c_i G_s(x_j; x_i) \tag{35}$$

is the lowest-order term in $v(x)$ and $\bar{v}$ dependent on the mutual trap positions. The MFPT minimization problem therefore can be studied, involving finding the globally optimal configuration of the N traps $x_1, \ldots, x_N \in \partial\Omega$. For the spherical domain, the constants $b_j = -c_j\kappa_j$ can be computed explicitly [4]. For the unit sphere with N equal traps, the "interaction energy" is given by (3).

Formulas (33) and (34) are useful for providing insights into the asymptotic expansion structure of the MFPT and the average MFPT. In order to employ these higher-order formulas for MFPT computation for a specific non-spherical domain, one additionally needs to derive exact or approximate explicit expressions for the Green's functions $G_s(x; x_j)$ and the constants b_j. Importantly, the lower-order two-term approximation (21) is ready to use in practical computations, since it only involves known quantities.

5 Discussion and Conclusions

The current paper aims to widen the body of results for the narrow escape problem (1) in three dimensions, by considering a general class of three-dimensional domains with N non-equal small well-separated boundary traps. This class of domains is described as the volume enclosed in a curvilinear coordinate level set of an orthogonal coordinate system, as discussed in Section 2.1. Using the method of matched asymptotic expansions, and utilizing the expansion of the surface Neumann Green's function of [17], in Section 2, we determined the two-term asymptotic expansion for the average mean first passage time for this class of domains. The average MFPT is given by formula (21); it involves the mean curvature of the domain boundary computed at the centers of the small i^{th} trap, and directly generalizes the results of [17] on the case of several traps, as well as the results of [4] for the unit sphere onto non-spherical domains. The derivation assumes the absence of the term of order $\varepsilon \log \frac{\varepsilon}{2}$ in the asymptotic expansion of the surface Neumann Green's function. While this assumption obviously holds for the unit sphere, and the comparison with a full numerical simulation suggests that this is the case for some non-spherical domains, it remains an open problem to present a rigorous argument to support or refute the above assumption for particular domain classes. In the cases where the assumption would not hold, the procedure developed in the current paper may be adjusted to accommodate for the non-zero $\varepsilon \log \frac{\varepsilon}{2}$ term.

In order to verify the two-term asymptotic expansion of the average MFPT, in Section 3, we performed several full finite-element numerical calculations of the average MFPT using COMSOL Multiphysics. These numerical calculations were done for three distinct domains – an oblate spheroid, a prolate spheroid, and a biconcave disk. For each such domain we considered an arrangements of $N = 3$ and $N = 5$ traps of different relative radii. The two-term asymptotic expansion of the average MFPT was found to be in close agreement with the full numerical calculations for small values of ε in each domain.

The form of a higher-order asymptotic expansion of the MFPT $v(x)$ (33) and the average MFPT $\bar{v}$ (34), parallel to that for the unit sphere, were computed for the considered class of domains in Section 4, assuming the far-field behaviour (31), (32). The higher-order terms involve a "trap interaction energy" term depending on mutual trap locations and the Green's function matrix. It is another open problem to solve the BVP for the w_2 term outlined in Appendix A,

in order to determine the unknown constants b_j in the formulas (33), (34).

When the trap interaction term for non-spherical domains is better understood, it would be a natural future work direction to study the global optimization of the average MFPT with respect to locations of a prescribed set of traps.

References

[1] P. C. Bressloff and J. M. Newby. Stochastic models of intracellular transport. *Reviews of Modern Physics*, 85(1):135, 2013.

[2] X. Chen and A. Friedman. Asymptotic analysis for the narrow escape problem. *SIAM Journal on Mathematical Analysis*, 43(6):2542–2563, 2011.

[3] A. F. Cheviakov, A. S. Reimer, and M. J. Ward. Mathematical modeling and numerical computation of narrow escape problems. *Physical Review E*, 85(2):021131, 2012.

[4] A. F. Cheviakov, M. J. Ward, and R. Straube. An asymptotic analysis of the mean first passage time for narrow escape problems. II. The sphere. *Multiscale Model. Simul.*, 8(3):836–870, 2010.

[5] A. F. Cheviakov and D. Zawada. Narrow-escape problem for the unit sphere: Homogenization limit, optimal arrangements of large numbers of traps, and the n 2 conjecture. *Physical Review E*, 87(4):042118, 2013.

[6] H. Cohn and A. Kumar. Universally optimal distribution of points on spheres. *Journal of the American Mathematical Society*, 20(1):99–148, 2007.

[7] A. B. Efimov and V. N. Vorob′ev. A mixed boundary-value problem for the Laplace equation. *Inž.-Fiz. Ž.*, 26(5):944–947, 1974.

[8] S. A. Gorski, M. Dundr, and T. Misteli. The road much traveled: trafficking in the cell nucleus. *Current opinion in cell biology*, 18(3):284–290, 2006.

[9] I. V. Grigoriev, Y. A. Makhnovskii, A. M. Berezhkovskii, and V. Y. Zitserman. Kinetics of escape through a small hole. *The Journal of chemical physics*, 116(22):9574–9577, 2002.

[10] D. Holcman and Z. Schuss. Escape through a small opening: receptor trafficking in a synaptic membrane. *J. Statist. Phys.*, 117(5-6):975–1014, 2004.

[11] S. Pillay, M. J. Ward, A. Peirce, and T. Kolokolnikov. An asymptotic analysis of the mean first passage time for narrow escape problems. I. Two-dimensional domains. *Multiscale Model. Simul.*, 8(3):803–835, 2010.

[12] C. Pozrikidis. Numerical simulation of the flow-induced deformation of red blood cells. *Annals of Biomedical Engineering*, 31(10):1194–1205, 2003.

[13] E. Rakhmanov, E. Saff, and Y. Zhou. Minimal discrete energy on the sphere. *Math. Res. Lett*, 1(6):647–662, 1994.

[14] Z. Schuss. *Theory and applications of stochastic differential equations.* John Wiley & Sons Inc., New York, 1980. Wiley Series in Probability and Statistics.

[15] A. Singer, Z. Schuss, and D. Holcman. Narrow escape. II. The circular disk. *J. Stat. Phys.*, 122(3):465–489, 2006.

[16] A. Singer, Z. Schuss, and D. Holcman. Narrow escape. III. Non-smooth domains and Riemann surfaces. *J. Stat. Phys.*, 122(3):491–509, 2006.

[17] A. Singer, Z. Schuss, and D. Holcman. Narrow escape and leakage of Brownian particles. *Phys. Rev. E (3)*, 78(5):051111, 8, 2008.

[18] A. Singer, Z. Schuss, D. Holcman, and R. S. Eisenberg. Narrow escape. I. *J. Stat. Phys.*, 122(3):437–463, 2006.

A The w_2 Problem

To continue the analysis we must consider the problem for w_2. We begin by observing that the terms appearing in the near-field expansion of v_2 do not contribute any $\mathcal{O}(1)$ terms because of the $\log \frac{\varepsilon}{2}$ term. Thus the far-field behaviour of w_2 can be determined by the $\mathcal{O}(1)$ terms already appearing in the matching condition (19). We find that w_2 must have the far field behaviour

$$w_2 \sim -2\pi v_0 c_j g_0 + B_j + \chi_1.$$

On the other hand, w_2 must satisfy the problem

$$\begin{aligned} \Delta_{(\eta,s_1,s_2)} w_2 &= v_0 \mathcal{L}_\Delta w_c, && \eta \geq 0, && s_1, s_2 \in \mathbb{R} \\ \partial_\eta w_2 &= 0, && \eta = 0, && s_1^2 + s_2^2 \geq a_j^2, \\ w_2 &= 0, && \eta = 0, && s_1^2 + s_2^2 \leq a_j^2. \end{aligned} \tag{36}$$

We decompose w_2 as

$$w_2 = (B_j + \chi_1)(1 - w_c) + w_{2p} + w_{2h},$$

where w_c is given by the solution to the electrified disk problem, w_{2p} satisfies the inhomogeneous PDE

$$\Delta_{(\eta,s_1,s_2)} w_{2p} = v_0 \mathcal{L}_\Delta w_c,$$

and w_{2h} satisfies

$$\begin{aligned} \Delta_{(\eta,s_1,s_2)} w_{2h} &= 0, && \eta \geq 0, && s_1, s_2 \in \mathbb{R} \\ \partial_\eta w_{2h} &= -\partial_\eta w_{2p}, && \eta = 0, && s_1^2 + s_2^2 \geq a_j^2, \\ w_{2h} &= -w_{2p}, && \eta = 0, && s_1^2 + s_2^2 \leq a_j^2. \end{aligned} \tag{37}$$

Theorem A.1. *The solution w_{2p} to the inhomogeneous problem is given by*

$$\begin{aligned} w_{2p} = \frac{v_0}{4} \quad & \left\{ \left[(2\lambda_\eta + \Lambda_{s_1}^\eta + \Lambda_{s_2}^\eta - \Lambda_\eta^\eta)\eta + (2\lambda_{s_1} + \Lambda_\eta^{s_1} + \Lambda_{s_2}^{s_1} - \Lambda_{s_1}^{s_1}) s_1 + (2\lambda_{s_2} + \Lambda_\eta^{s_2} + \Lambda_{s_1}^{s_2} - \Lambda_{s_2}^{s_2}) s_2 \right] w_c \right. \\ & + \left[\Lambda_\eta^\eta \eta^2 + 2\Lambda_\eta^{s_1} \eta s_1 + 2\Lambda_\eta^{s_2} \eta s_2 - \Lambda_{s_1}^\eta s_1^2 - \Lambda_{s_2}^\eta s_2^2 \right] \frac{\partial w_c}{\partial \eta} \\ & + \left[\Lambda_{s_1}^{s_1} s_1^2 + 2\Lambda_{s_1}^\eta \eta s_1 + 2\Lambda_{s_1}^{s_2} s_1 s_2 - \Lambda_\eta^{s_1} \eta^2 - \Lambda_{s_2}^{s_1} s_2^2 \right] \frac{\partial w_c}{\partial s_1} \\ & \left. + \left[\Lambda_{s_2}^{s_2} s_2^2 + 2\Lambda_{s_2}^\eta \eta s_2 + 2\Lambda_{s_2}^{s_1} s_1 s_2 - \Lambda_\eta^{s_2} \eta^2 - \Lambda_{s_1}^{s_2} s_1^2 \right] \frac{\partial w_c}{\partial s_2} \right\} \end{aligned} \tag{38}$$

Proof. We begin by defining the three functions with unknown constant coefficients

$$\Phi_A^\eta = A_1^\eta \eta^2 \frac{\partial w_c}{\partial \eta} + A_2^\eta \eta w_c, \qquad \Phi_B^\eta = B_1^\eta \eta^2 \frac{\partial w_c}{\partial s_1} + B_2^\eta \eta s_1 \frac{\partial w_c}{\partial \eta}, \qquad \Phi_C^\eta = C_1^\eta \eta^2 \frac{\partial w_c}{\partial s_2} + C_2^\eta \eta s_2 \frac{\partial w_c}{\partial \eta}.$$

A straightforward calculation using the fact that $\dfrac{\partial^2 w_c}{\partial \eta^2} = -\dfrac{\partial^2 w_c}{\partial s_1^2} - \dfrac{\partial^2 w_c}{\partial s_2^2}$ results in

$$\begin{aligned}
\Delta_{(\eta,s_1,s_2)} \Phi_A^\eta &= 4A_1^\eta \eta \frac{\partial^2 w_c}{\partial \eta^2} + 2(A_1^\eta + A_2^\eta) \frac{\partial w_c}{\partial \eta} \\
\Delta_{(\eta,s_1,s_2)} \Phi_B^\eta &= 2B_2^\eta s_1 \frac{\partial^2 w_c}{\partial \eta^2} + (4B_1^\eta + 2B_2^\eta)\eta \frac{\partial^2 w_c}{\partial \eta \partial s_1} + 2B_1^\eta \frac{\partial w_c}{\partial s_1}, \\
\Delta_{(\eta,s_1,s_2)} \Phi_C^\eta &= 2C_2^\eta s_2 \frac{\partial^2 w_c}{\partial \eta^2} + (4C_1^\eta + 2C_2^\eta)\eta \frac{\partial^2 w_c}{\partial \eta \partial s_2} + 2C_1^\eta \frac{\partial w_c}{\partial s_2}.
\end{aligned}$$

Setting $A_1^\eta = \dfrac{v_0 \Lambda_\eta^\eta}{4}$, $B_2^\eta = \dfrac{v_0 \Lambda_\eta^{s_1}}{2}$, $C_2^\eta = \dfrac{v_0 \Lambda_\eta^{s_2}}{2}$, as well as $B_1^\eta = -\dfrac{1}{2} B_2^\eta$ and $C_1^\eta = -\dfrac{1}{2} C_2^\eta$ we find that

$$\Delta_{(\eta,s_1,s_2)}(\Phi_A^\eta + \Phi_B^\eta + \Phi_C^\eta) = v_0 \left[\Lambda_\eta \frac{\partial^2 w_c}{\partial \eta^2} + \frac{1}{2}(\Lambda_\eta^\eta + 4A_2^\eta) \frac{\partial w_c}{\partial \eta} - \frac{1}{2} \Lambda_\eta^{s_1} \frac{\partial w_c}{\partial s_1} - \frac{1}{2} \Lambda_\eta^{s_2} \frac{\partial w_c}{\partial s_2} \right].$$

Using the same argument but this time permuting η, s_1, and s_2 we find that

$$\begin{aligned}
\Delta_{(\eta,s_1,s_2)}(\Phi_A^{s_1} + \Phi_B^{s_1} + \Phi_C^{s_1}) &= v_0 \left[\Lambda_{s_1} \frac{\partial^2 w_c}{\partial s_1^2} + \frac{1}{2}(\Lambda_{s_1}^{s_1} + 4A_2^{s_1}) \frac{\partial w_c}{\partial s_1} - \frac{1}{2} \Lambda_{s_1}^\eta \frac{\partial w_c}{\partial \eta} - \frac{1}{2} \Lambda_{s_1}^{s_2} \frac{\partial w_c}{\partial s_2} \right], \\
\Delta_{(\eta,s_1,s_2)}(\Phi_A^{s_2} + \Phi_B^{s_2} + \Phi_C^{s_2}) &= v_0 \left[\Lambda_{s_2} \frac{\partial^2 w_c}{\partial s_2^2} + \frac{1}{2}(\Lambda_{s_2}^{s_2} + 4A_2^{s_2}) \frac{\partial w_c}{\partial s_2} - \frac{1}{2} \Lambda_{s_2}^\eta \frac{\partial w_c}{\partial \eta} - \frac{1}{2} \Lambda_{s_2}^{s_1} \frac{\partial w_c}{\partial s_1} \right].
\end{aligned}$$

With $w_{2p} = \Phi_A^\eta + \Phi_B^\eta + \Phi_C^\eta + \Phi_A^{s_1} + \Phi_B^{s_1} + \Phi_C^{s_1} + \Phi_A^{s_2} + \Phi_B^{s_2} + \Phi_C^{s_2}$ we find that

$$\begin{aligned}
\Delta_{(\eta,s_1,s_2)} w_{2p} = v_0 \Bigg[& \Lambda_\eta \frac{\partial^2 w_c}{\partial \eta^2} + \Lambda_{s_1} \frac{\partial^2 w_c}{\partial s_1^2} + \Lambda_{s_2} \frac{\partial^2 w_c}{\partial s_2^2} + \frac{1}{2}(\Lambda_\eta^\eta + 4A_2^\eta - \Lambda_{s_1}^\eta - \Lambda_{s_2}^\eta) \frac{\partial w_c}{\partial \eta} \\
& + \frac{1}{2}(\Lambda_{s_1}^{s_1} + 4A_2^{s_1} - \Lambda_\eta^{s_1} - \Lambda_{s_2}^{s_1}) \frac{\partial w_c}{\partial s_1} + \frac{1}{2}(\Lambda_{s_2}^{s_2} + 4A_2^{s_2} - \Lambda_\eta^{s_2} - \Lambda_{s_1}^{s_2}) \frac{\partial w_c}{\partial s_2} \Bigg].
\end{aligned}$$

Finally the coefficients of $\dfrac{\partial w_c}{\partial \eta}$, $\dfrac{\partial w_c}{\partial s_1}$, and $\dfrac{\partial w_c}{\partial s_2}$ are set to zero by choosing A_2^η, $A_2^{s_1}$, and $A_2^{s_2}$ accordingly which yields the desired result (38). □

With the result for w_{2p} above, we can explicitly write out the boundary conditions for w_{2h} as

$$w_{2h}|_{\eta=0} = -\frac{v_0}{4} \left[(2\lambda_{s_1} + \Lambda_\eta^{s_1} + \Lambda_{s_2}^{s_1} - \Lambda_{s_1}^{s_1}) s_1 + (2\lambda_{s_2} + \Lambda_\eta^{s_2} + \Lambda_{s_1}^{s_2} - \Lambda_{s_2}^{s_2}) s_2 - (\Lambda_\eta^{s_1} s_1^2 + \Lambda_\eta^{s_2} s_2^2) \frac{\partial w_c}{\partial \eta}|_{\eta=0} \right]$$

for $s_1^2 + s_2^2 < a_j^2$, and

$$\partial_\eta w_{2h}|_{\eta=0} = -\frac{v_0}{4} \left[(2\lambda_\eta + \Lambda_{s_1}^\eta + \Lambda_{s_2}^\eta - \Lambda_\eta^\eta) w_c|_{\eta=0} - (\Lambda_{s_1}^\eta s_1^2 + \Lambda_{s_2}^\eta s_2^2) \frac{\partial^2 w_c}{\partial \eta^2}|_{\eta=0} + 2\Lambda_{s_1}^\eta s_1 \frac{\partial w_c}{\partial s_1}|_{\eta=0} + \frac{v_0}{2} \Lambda_{s_2}^\eta s_2 \frac{\partial w_c}{\partial s_2}|_{\eta=0} \right]$$

for $s_1^2 + s_2^2 > a_j^2$. It may be possible to express the solution to the problem for w_{2h} in terms of the Green's functions obtained using the Sommerfeld method, as outlined in [7].